Appendix

An essential step of kinetochore formation controlled by the SNARE protein Snap29

Table of Contents

Appendix Table S1: List of *Drosophila* genotypes for the *in vivo* experiments.

Panel	Label	Genotype
Figure 2A	control	MS1096 Gal4>; +/+; +/+; +/+
	Mis12 RNAi	MS1096 Gal4> ; ; UAS Mis12 RNAi/+
	Spc105 RNAi	MS1096 Gal4>; ;UAS Spc105 RNAi/+
	Ndc80 RNAi	MS1096 Gal4> ;UAS Ndc80 RNAi/+;
	Nuf2 RNAi	MS1096 Gal4>; UAS Nuf2 RNAi/+;
	Zw10 RNAi	MS1096 Gal4>; ;UAS Zw10 RNAi/+
Figure 2C	Snap29 RNAi	MS1096 Gal4>; UAS Snap29 RNAi/+;
	Snap29 RNAi + NPFAAA	MS1096 Gal4>; UAS Snap29 RNAi/+; UAS NPFAAA /+
	Snap29 RNAi + ΔSNARE1	MS1096 Gal4>; UAS Snap29 RNAi/+; UAS ΔSNARE1/+
	Snap29 RNAi + ΔSNARE2	MS1096 Gal4>; UAS Snap29 RNAi/+; UAS ΔSNARE2/+
Figure 7A, C, D, E	Wild-type	w; FRT42, GMR-Hid/+; eyGal4, UASFLP/+
Figure 7B, C, D, F	Snap29 mutant	w; FRT42, GMR-Hid/ FRT42 B6-21; eyGal4, UASFLP/+
Figure 7G	p35	w; FRT42, GMR-Hid/+; eyGal4, UASFLP/UAS p35
Figure 7H	Snap29 m. + p35	w; FRT42, GMR-Hid/ FRT42 B6-21; eyGal4, UASFLP/UAS p35
Figure S7A, C	Wild-type	w; FRT42, GMR-Hid/+; eyGal4, UASFLP/+
Figure S7B, D	Snap29 mutant	w; FRT42, GMR-Hid/ FRT42 B6-21; eyGal4, UASFLP/+
Figure S7E	Wild-type	yw
	Syx17/ Df	;;Syx17LL06330/ Df(3L)Exel8098
	Vamp7/ Df	;;Vamp7G7738/ Df(2R)BSC132.

Figure S7G, H	Snap29 m. + p35	w; FRT42, GMR-Hid/ FRT42 B6-21; eyGal4, UASFLP/UAS p35 (allograft); w-; His2Av-mRFP(Host)
Figure S8A-B	Control or TJ>	; traffic jam-Gal4/+;
Figure S8C	TJ> dsSnap29	; traffic jam-Gal4/UAS Snap29 RNAi;

Appendix figures

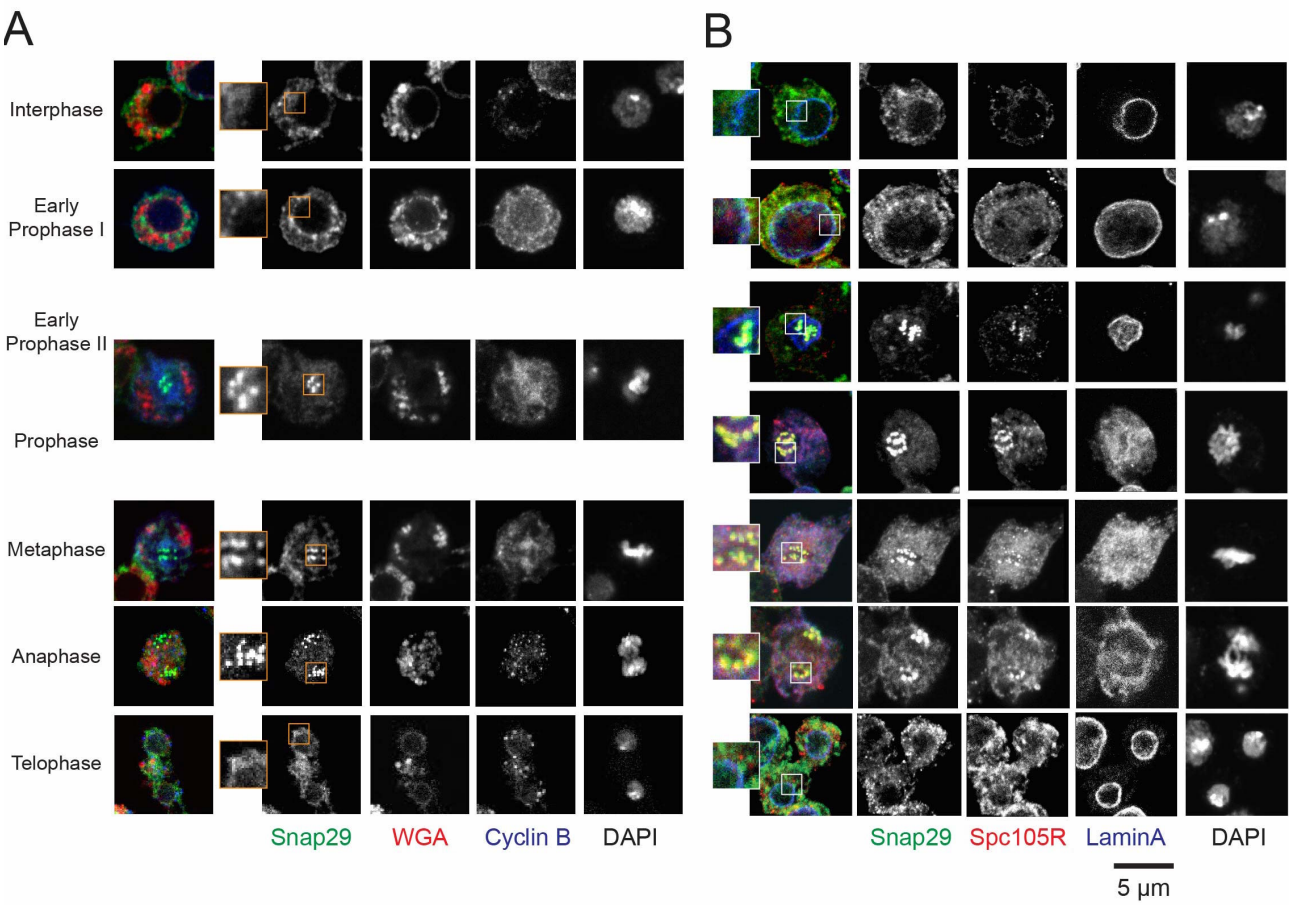

Appendix Fig. S1: Snap29 localization in *Drosophila* S2 cells.

(A-B) Single confocal sections of S2 cells at the indicated mitotic stages stained to detect Snap29, nuclear pores (WGA) CyclinB and the DNA (DAPI) (A), or Snap29, Spc105R, and the nuclear envelope (LaminA) and the DNA (B).

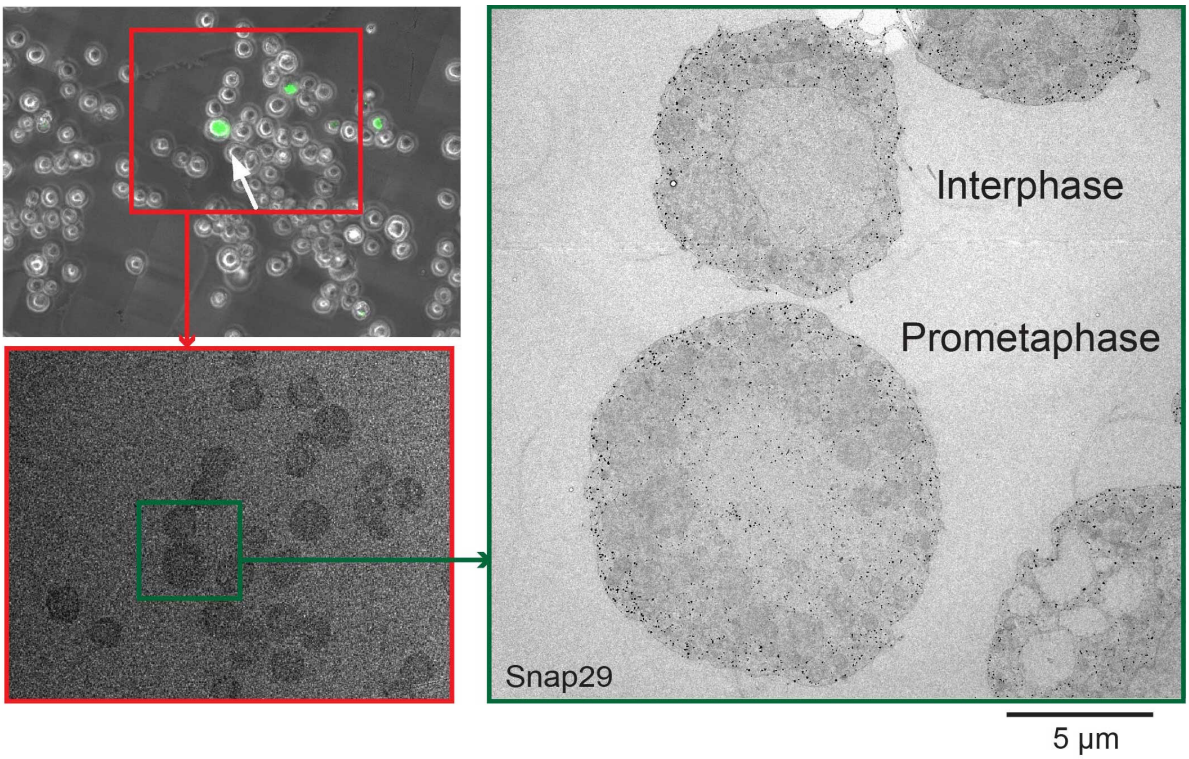

Appendix Fig. S2: Snap29 localization in *Drosophila* S2 cells by CLEM.

Identification of mitotic cells for CLEM was performed by staining with anti-pH3 cells permeabilized mildly in 0.5 % Saponin to preserve membranes. The cell presented in the right panel is highlighted by the white arrow in the upper left panel.

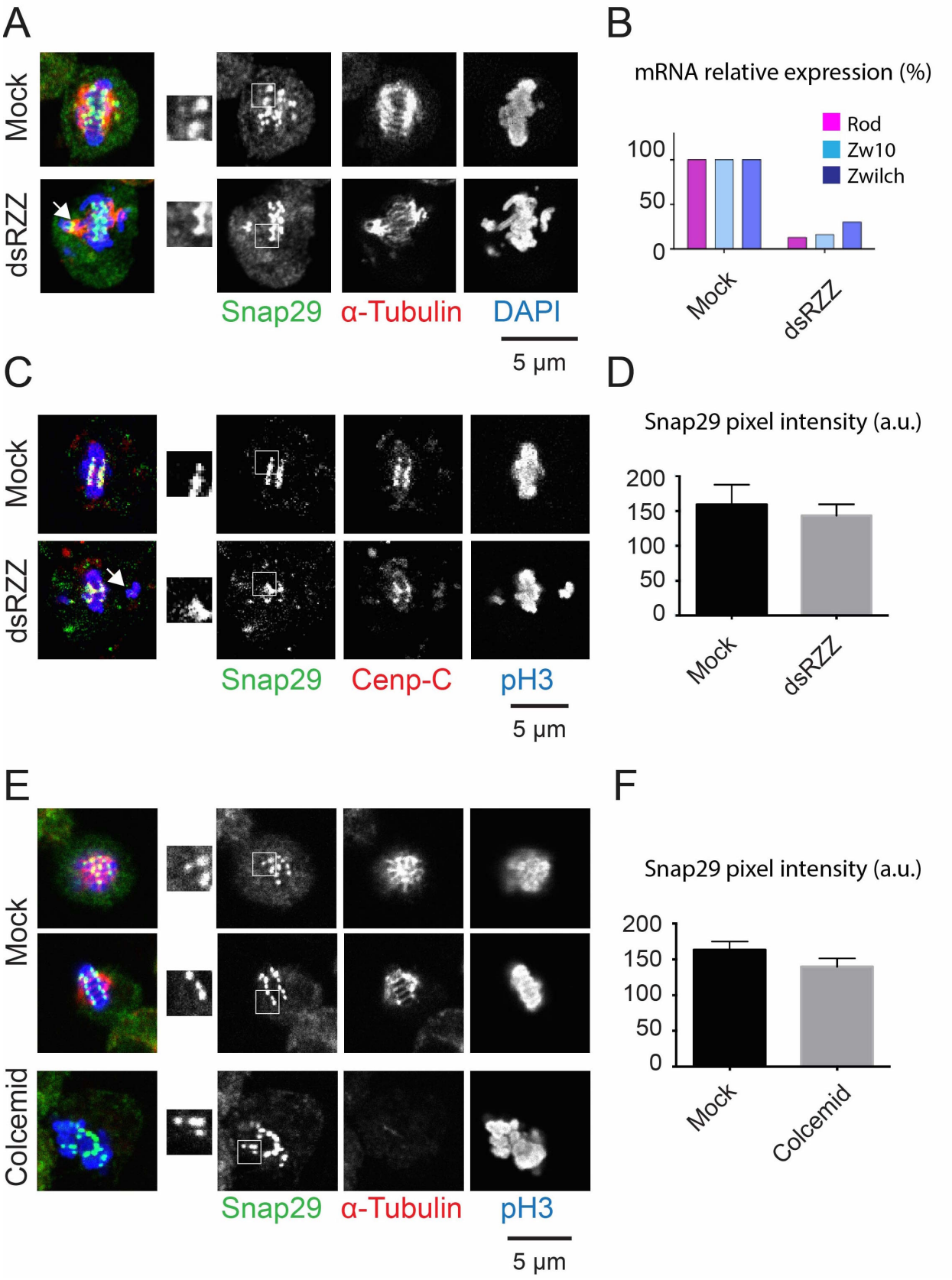
A
Mock
dsRZZ
Snap29
α-Tubulin
DAPI
5 μm
B
mRNA relative expression (%)
Rod
Zw10
Zwilch
100
50
0
Mock
dsRZZ
C
Mock
dsRZZ
Snap29
Cenp-C
pH3
5 μm
D
Snap29 pixel intensity (a.u.)
200
150
100
50
0
Mock
dsRZZ
E
Mock
Colcemid
Snap29
α-Tubulin
pH3
5 μm
F
Snap29 pixel intensity (a.u.)
200
150
100
50
0
Mock
Colcemid

Appendix Fig. S3: Requirements for Snap29 localization to KTs in S2 cells.

(A, C) Single confocal sections of S2 cells at metaphase mock-treated or treated to down-regulate simultaneously Zw10, Zwilch and Rod (dsRZZ). Arrowheads point to chromosome congression defects, indicating the effectiveness of knock-downs. (B) Quantification of Zw10, Zwilch and Rod expression by Q-PCR. (D) Quantification of Snap29 signal in the experiment in panel c considering 3 experiments. (E) Single confocal section of a cell treated with 0.5µg/ml colcemid to depolymerize MTs. (F) Quantification of Snap29 signal in the experiment in panel e considering 3 experiments. In both quantification graphs (D, F), P values by unpaired t-test indicate non significant differences.

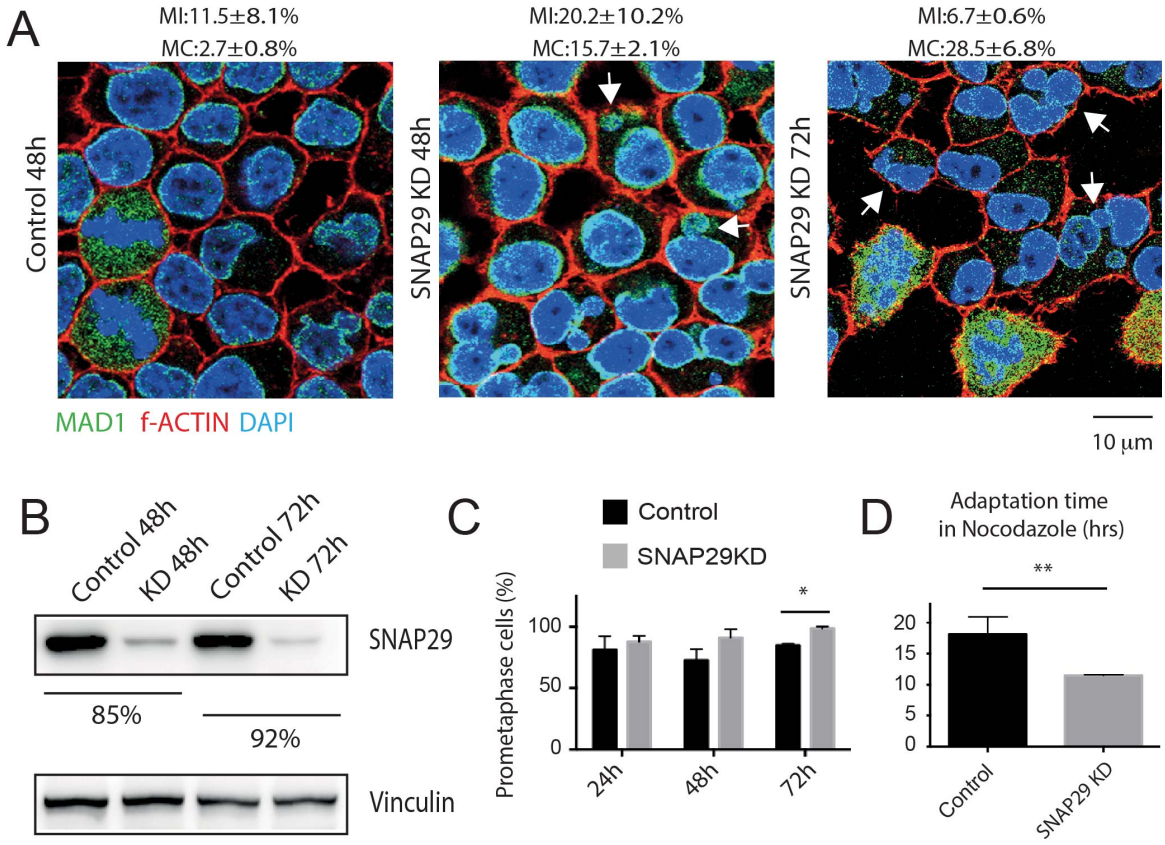

Appendix Fig. S4: The effects of SNAP29 depletion in HeLa cells.

(A) Single confocal sections of populations of HeLa cells stained with anti-MAD1 to label the nuclear envelope in interphase, Phalloidin to visualize the f-actin cytoskeleton and DAPI. The mitotic index (MI: mean of 3 experiments ±SD) and the percentage of cells with multiple micronuclei (arrows; MC: mean of 3 experiments ±SD) is shown. (B) Immunoblotting of HeLa protein extracts, relative to the experiments in a. Percentages indicate SNAP29 protein reduction. (C) Quantification of the experiment in a-b, showing the number of cells at the indicated mitotic stage in control and SNAP29 KD cells, based on 3 independent experiments. The P value is obtained by multiple t-test. (D) Quantification of the average time at which individual cells exit mitosis upon treatment with Nocodazole, based on 3 experiments in each of which 50 cells/sample were recorded by time-lapse microscopy for 48 hrs. The P values is obtained by unpaired t-test.

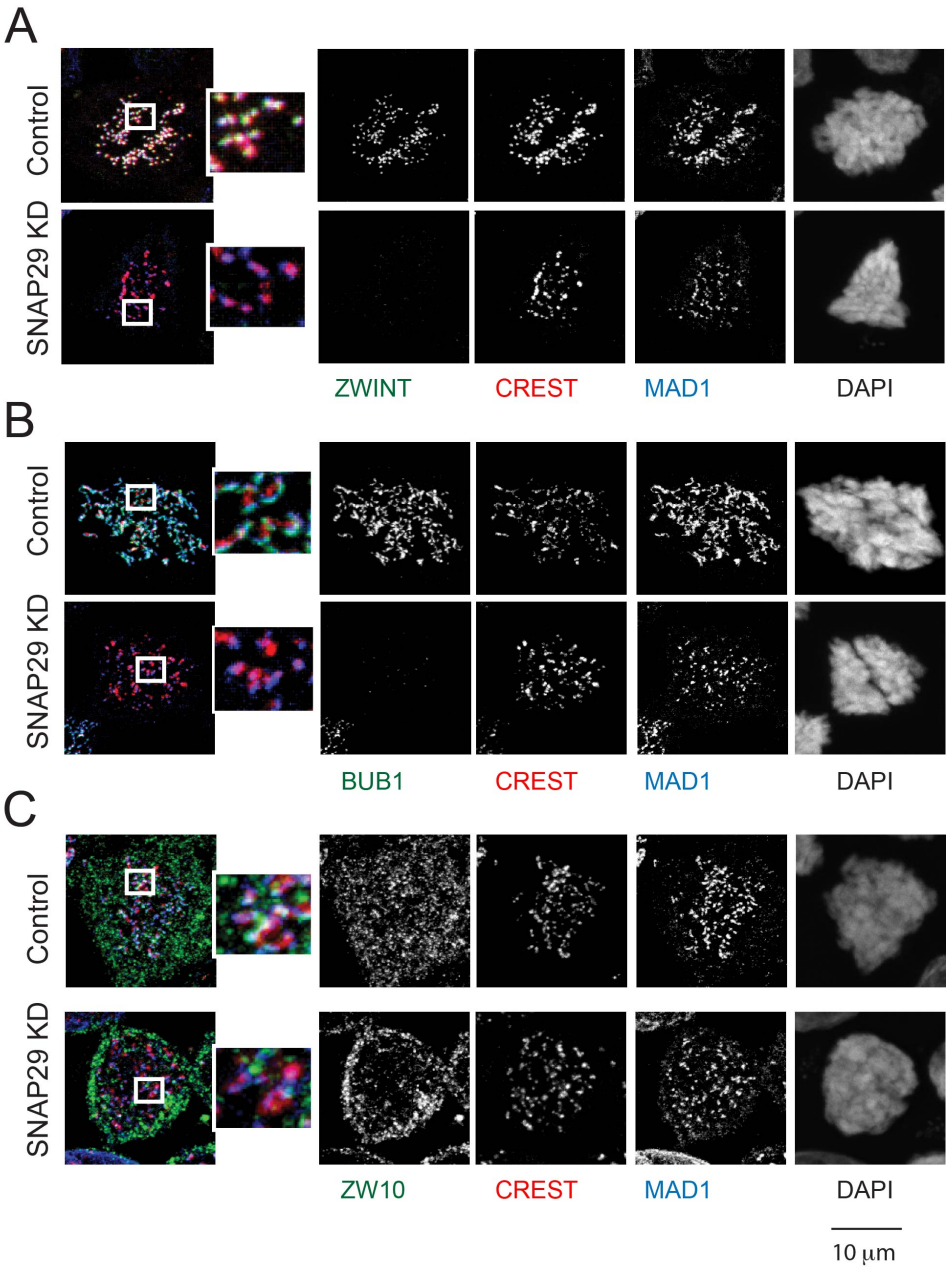

Appendix Fig. S5: MAD1 localization at KTs relative to ZWINT, BUB1 and ZW10 in control and SNAP29 depleted HeLa cells.

(A-C) Max projection of single control and SNAP29 KD HeLa cells treated as in Fig. 5. Enlargements of boxed areas are shown to highlight localizations of the indicated proteins to KTs.

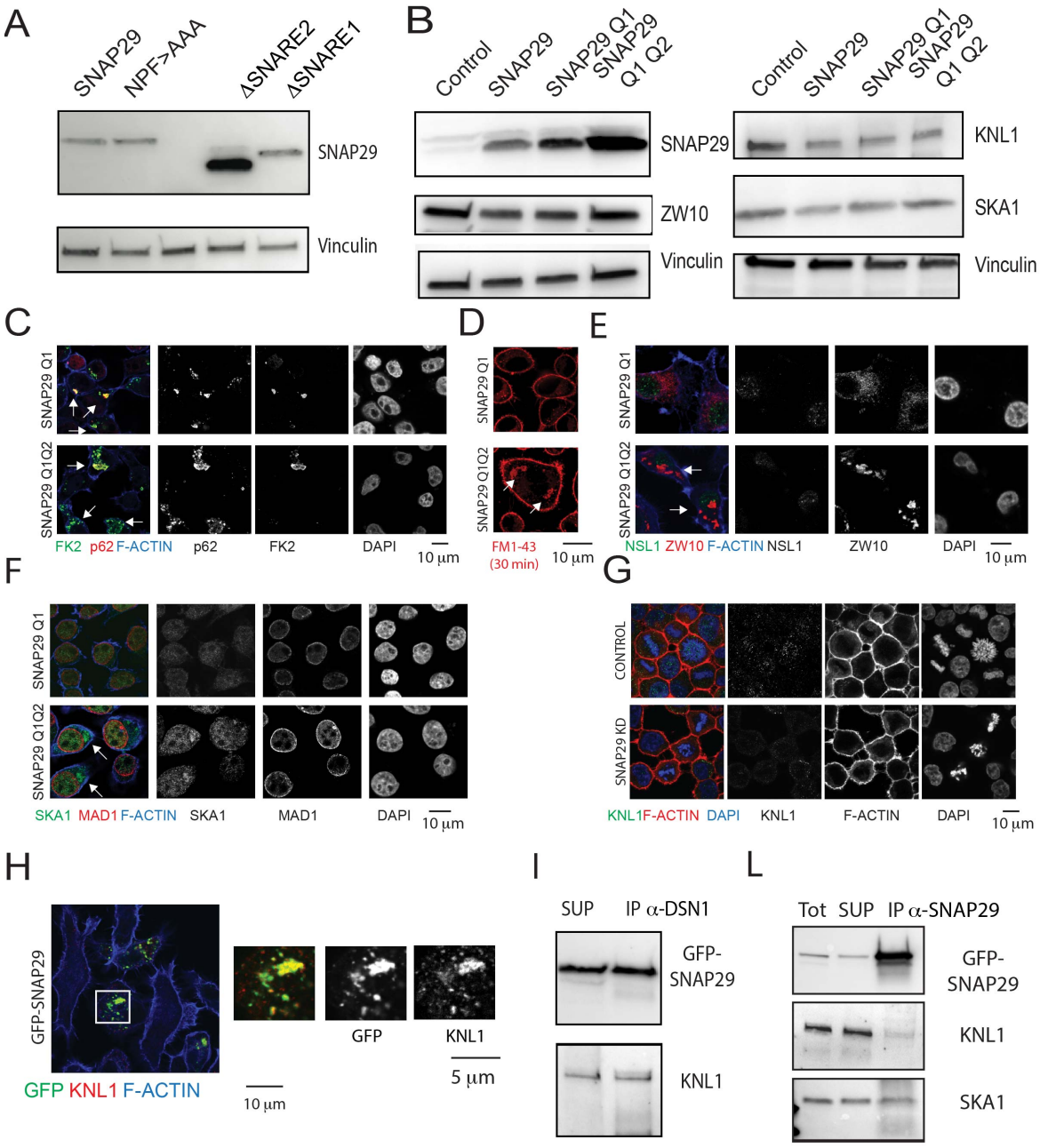

Appendix Fig. S6: Expression of SNAP29 forms in HeLa cells.

(A-B) Western blot of extracts of HeLa cells expressing the indicated SNAP29 forms, relative to the experiment in Fig. 6. (C-F) Single confocal sections of HeLa cells in interphase overexpressing the indicated construct. Cells expressing SNAP29 Q1 Q2 display accumulations of p62 that are often positive for ubiquitin (C, arrows), and of ZW10 (E, arrows) and SKA1 (F arrows) but not of NSL1 (E) and MAD1 (F). These could represent aberrant membranes compartments, as revealed

by incorporations of the lipophilic dye FM1-43 (D, arrows). (G) Single confocal sections of HeLa cells treated as indicated. SNAP29 depletion does not cause accumulation of KNL1. (H) Single confocal section of HeLa cells in interphase overexpressing GFP-SNAP29, which colocalizes with KNL1 in cytoplasmic accumulations. Single channels are shown in insets of the boxed area. (I-L) Immunoblotting of HeLa cells extracts transfected with GFP-SNAP29 and immunoprecipitated with the indicated antibody. KNL1 and GFP-SNAP29 are in complex with DSN1 (I) and KNL1 and SKA1 are in complex with SNAP29 (L), in agreement with previous identification by Mass Spec of SNAP29 peptides in SKA1 immuno-precitations (Welburn, Grishchuk et al., 2009). SUP: Supernatant; IP: Immunoprecipitate

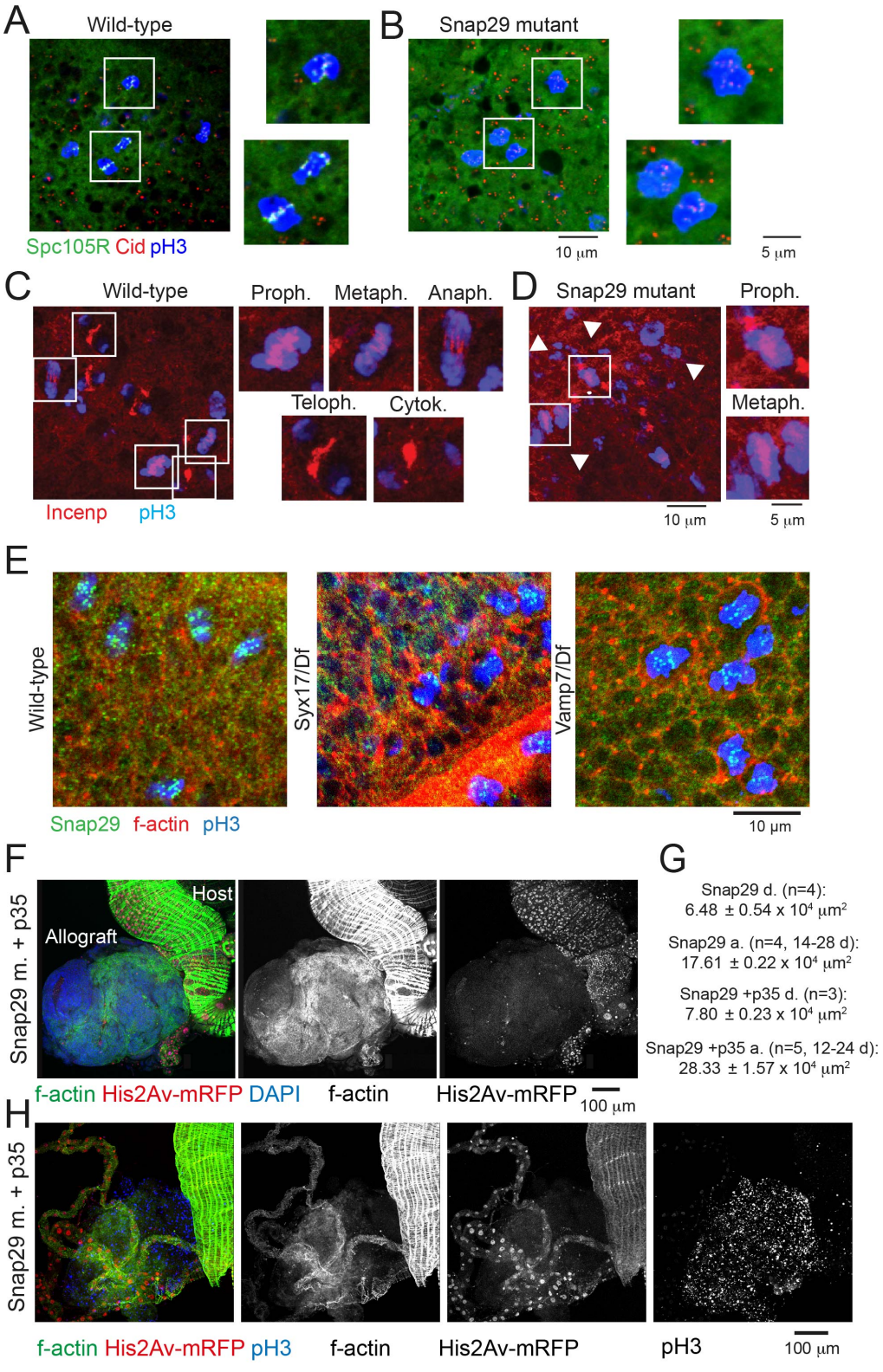

Appendix Fig. S7: Snap29 localization and function in eye imaginal discs.

(A-D) High magnifications of a confocal cross-sections of portions of wild-type and Snap29 mutant eye disc tissue anterior to the morphogenetic furrow of third instar

larvae. Cid and Spc105R mark the inner and outer KT, respectively (A-B and insets), while Incenp relocalizes to the spindle mid-zone during anaphase allowing identification of mitotic phases (C-D and insets). Arrowheads in D point to fragmented DNA. (E) Analysis of Snap29 localization at KT of Syx17 and Vamp7 mutants compared to wild type eye imaginal discs. Single confocal cross-sections of a portion of the eye imaginal discs anterior to the morphogenic furrow are shown. Proliferating cells and f-actin are marked with anti-pH3 antibody and phalloidin. (F, H) Single confocal sections of allografted tissue dissected from the abdomen of female hosts expressing His2Av-mRFP. The tumor tissue is identified by lack of mRFP expression, which is otherwise clearly visible in the gut of the host. The allografted tumor tissue contains many pH3-positive cells, indicating the presence of dividing cells (H). (G) Quantification of the average area of medial microscopic sections of the indicated tissue (d.=donor, a.=allograft) suggests that the transplanted tissue is able to grow within the host.

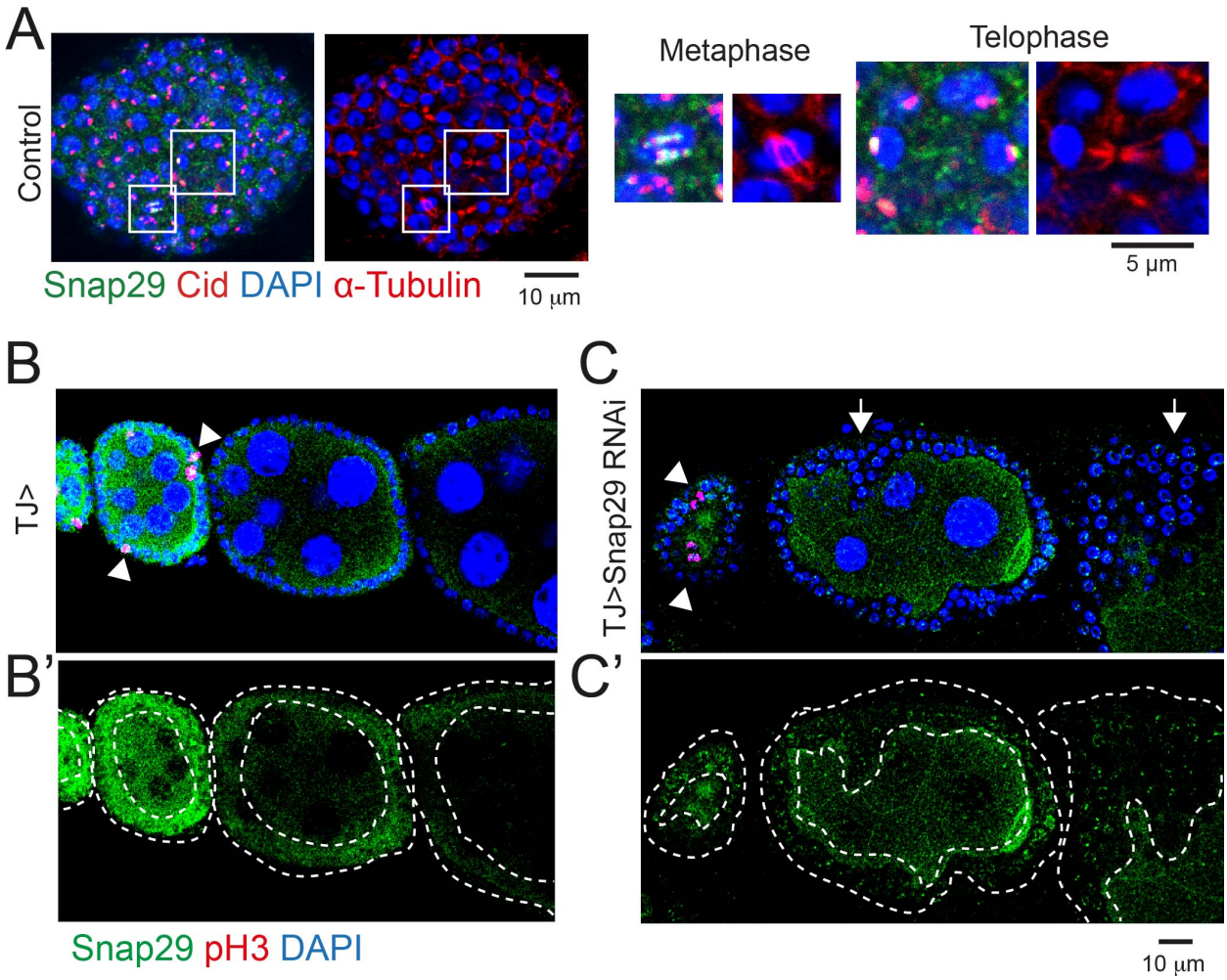

Appendix Fig. S8. Snap29 localization and function in follicular cells.

(A) Single confocal sections of a *Drosophila* stage 5-6 egg chamber dissected form the ovary of 3 days-old mated and well-fed females. A basal section through the follicular epithelium is shown for Snap29, Cid and DNA labeling (left), and for α-tubulin and DNA labeling (right). Enlargement of the insets are shown on the right. (B-C) Cross-sections through stage 5 to 8 egg chambers belonging to individual ovarioles, expressing dsRNA against Snap29 using the driver traffic jam-GAL4 (TJ>). Tissues are stained with anti-Snap29, anti-pH3 to mark proliferating cells and with DAPI to mark nuclei. Arrowheads highlight the Snap29 signal of dividing cells (B) which is lost upon depletion of Snap29 (C). Single Snap29 channels in b'-c' show reduction of Snap29 expression specifically in the follicular epithelium in which trafficjam-GAL4 is expressed (outlined by the broken lines). Snap29 down regulation correlates with severe multi-layering of the epithelial monolayer (arrows in C), compared to control (B).

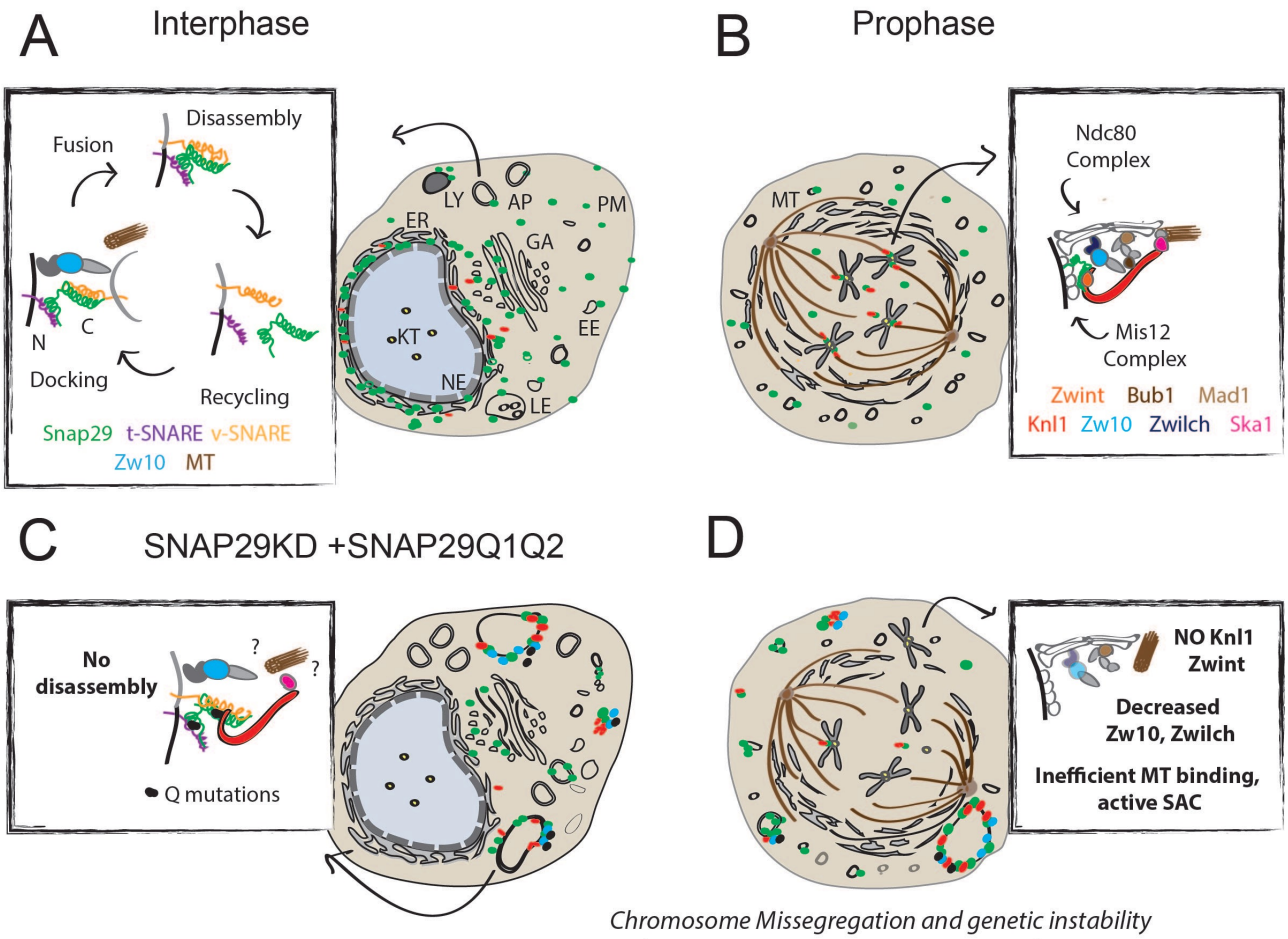

Chromosome Missegregation and genetic instability contributing to tumorigenesis upon escape from apoptosis

Appendix Fig. S9. A model for SNARE function at the KT.

(Aa) In interphase cells, Snap29 is found localized to the cytoplasm and to a wide range of membrane compartments, such as autophagosomes (AP), early and late endosomes (EE and LE), lysosomes (LY), the plasma membrane (PM), the Golgi apparatus (GA) and the ER (see also (Morelli et al., 2014)). At membranes, Snap29 takes part in cycles of membrane fusion of incoming vesicles, usually docked to target membranes with the help of tethering complexes after MT-dependent transport. At the end of fusion, SNARE complex disassembly by the ATPase NSF and α-snap release VAMPs, that are recycled for subsequent rounds of fusion (inset). At the onset of mitosis, Snap29 is transiently enriched in proximity of the nuclear envelope (NE), which is continuous with the ER. At this stage Snap29 is excluded from the nucleoplasm. (B) In early prophase, Snap29 is recruited to KTs

together with Knl1, where they resides to the end of anaphase, stabilizing MT binding at the outer KT (inset). (C) When endogenous Snap29 is substituted with a form that cannot be disassembled from a SNARE complex (inset) Snap29 as well as Knl1, and possibly Zw10 and Ska1, are re-localized to trafficking compartments. (D) Under these conditions, in prophase Knl1 is not localized to KTs at the onset of mitosis, preventing correct MT binding (inset). In such cells, active but inefficient SAC response allows occasional chromosome mis-segregation and genetic instability, contributing to tumorigenesis upon escape from apoptosis.